EEET ECOLOGICAL ENGINEERING & ENVIRONMENTAL TECHNOLOGY

Ecological Engineering & Environmental Technology, 2026, 27(3), 401–414
https://doi.org/10.12912/27197050/218441
ISSN 2719–7050, License CC-BY 4.0

Received: 2026.01.22
Accepted: 2026.02.23
Published: 2026.03.01

Spatio temporal drought pattern analysis using vegetation health index and standardized precipitation index in Sragen Regency

Muhammad Afif Farhan[1], Bayu Dwi Apri Nugroho[2*], Much. Taufik Tri Hermawan[3], Afifatul Husna Al-Adilah[4]

[1] Program of Geo-Information for Spatial Planning and Disaster Risk Management, Universitas Gadjah Mada, Jl. Teknika Utara, Yogyakarta, 55284, Indonesia Universitas Gadjah Mada, Jl. Flora, Bulaksumur, Yogyakarta, 55281, Indonesia
[2] Department of Agriculture and Biosystem Engineering, Faculty of Agricultural Technology, Universitas Gadjah Mada, Jl. Flora, Bulaksumur, Yogyakarta, 55281, Indonesia
[3] Department of Forest Science, Faculty of Forestry, Universitas Gadjah Mada, Jl. Agro No. 1 Bulaksumur, Yogyakarta 55281, Indonesia
[4] Research Center of Land Resources Development, Universitas Gadjah Mada, Jl. Kuningan, Caturtunggal, Depok, Sleman, Yogyakarta 55281, Indonesia
* Corresponding author's e-mail: bayu.tep@ugm.ac.id

ABSTRACT

This study analyses the spatio temporal drought patterns in Sragen Regency, Central Java, by integrating meteorological and vegetation based indicators to evaluate climatic variability and its impact on agricultural productivity. Using standardized precipitation index (SPI) derived from 30 years CHIRPS precipitation data and vegetation health index (VHI) generated from Landsat 8 and 9 imagery, the analysis focused on three representative climatic periods, 2015 (El Niño), 2018 (Normal), and 2022 (La Niña), covering the dry season months of June to October. The results indicate that 2015 experienced the most severe drought, with extreme and severe drought areas increasing from 3,781 ha in June to 16,600 ha in October, corresponding to SPI values between -1.21 and -2.5 and a total drought affected area of approximately 46,000 ha (63%). During the 2018 normal period, extreme drought expanded from 512 ha to 2,359 ha, while severe drought peaked at 13,687 ha, covering around 56,300 ha (76%), reflecting moderate drought conditions due to partial rainfall recovery. Conversely, 2022 (La Niña) exhibited predominantly wet conditions, with extreme drought areas fluctuating between 28-324 ha, severe drought between 583-920 ha, and nondrought areas dominating over 63,000 ha (86%). Validation using rice harvest data showed a decline in 2015 (97,444 ha) compared to 100,492 ha in 2018 and 104,662 ha in 2022, aligning with drought intensity trends. Spatially, droughts were concentrated in the northern and central regions, characterized by rainfed paddy fields with limited irrigation infrastructure. Overall, the integration of SPI and VHI effectively captures both meteorological and agricultural drought dynamics, highlighting that El Niño amplifies drought severity while La Niña enhances vegetation recovery, thus emphasizing the potential of remote sensing indices in supporting drought early warning systems and adaptive agricultural management in Sragen Regency.

Keywords: agriculture; remote sensing; paddy field; vhi; spi; drought

INTRODUCTION

Drought represents a multifaceted environmental challenge that can lead to agricultural failures (Piao et al., 2010), nutritional deficits (Awasthi et al., 2024), widespread hunger (Gebre et al., 2021) and disease outbreaks (Asmall et al., 2021). Historical records demonstrate that intense drought periods have caused substantial adverse effects across both ecological and human systems (Bajrai, 2025). Consequently, there is a pressing need to enhance our comprehension of

how droughts develop spatially and temporally, along with their progression patterns (W. Yu et al., 2013). Drought dynamics knowledge would establish a foundation for measuring drought consequences and understanding how societies, economies, and ecosystems adapt to water scarcity across different geographical areas and time periods (Letsoalo et al., 2023).

Drought phenomena are generally classified into four distinct categories based on their primary characteristics: meteorological drought (characterized by reduced rainfall), agricultural or vegetation-based drought (marked by depleted soil water content), hydrological drought (defined by diminished surface water flow and underground water reserves), and socioeconomic drought (representing societal reactions to water availability versus requirements) (Junior, 2002). Vegetation based drought holds particular significance due to its direct relationship with agricultural productivity, and evidence suggests that the geographical scope of such drought conditions has been expanding (F.N. Kogan, 1997). Projections indicate that both the frequency and persistence of extreme drought conditions will continue rising (Wang et al., 2025). Developing effective methodologies to identify vegetation drought occurrences and assess long term drought vulnerability has become critical (Uddin et al., 2020). Drought monitoring tools could serve as valuable resources for decision makers seeking to deploy timely prevention and response measures (Senay et al., 2023).

One of the widely adopted meteorological drought indicator tools is the standard precipitation index (SPI), which quantifies precipitation deficits across multiple temporal scales (Guttman, 1999). The SPI is calculated by fitting precipitation data to a probability distribution, which is then transformed into a standardized normal distribution (Mupepi & Matsa, 2023), this standardization enables comparison of drought conditions across different geographical regions and climatic zones, regardless of local precipitation patterns (Mckee et al., 1993). SPI operates solely on precipitation data, making it relatively simple to compute and applicable in data scarce environments where other meteorological variables may not be readily available (Fentaw et al., 2023). The index can be calculated for various time periods ranging from one month to several years, allowing researchers to assess both short-term agricultural impacts and long-term hydrological drought conditions (Alahacoon & Amarnath, 2022).

Vegetation health index (VHI) ranks among the most widely utilized remote sensing based drought monitoring tools (Zeng et al., 2023). VHI combines two components: the Vegetation Condition Index (VCI) and the thermal condition index (TCI) (F. N. Kogan, 1995). This index accounts for regional biological and climatic characteristics, making it applicable for monitoring actual plant water stress across diverse agricultural and meteorological zones (Mupepi & Matsa, 2023). The foundational concepts underlying VHI include: (1) diminished Normalized Difference Vegetation Index (NDVI) (X. Yu & Guo, 2023) or enhanced vegetation index (EVI) values coupled with elevated Land Surface Temperature (LST) readings indicate compromised vegetation conditions (Amalo et al., 2017), and (2) VCI and TCI are weighted equally in the VHI calculation.

Given the complementary nature of meteorological and remotely sensed drought indices, integrating the Standard Precipitation Index with the Vegetation Health Index offers a comprehensive approach to agricultural drought assessment (Alahacoon & Amarnath, 2022). While SPI effectively captures meteorological drought conditions by quantifying precipitation anomalies, it does not directly reflect how vegetation responds to water stress (Bhaga et al., 2023). VHI provides real time information on actual vegetation health status through satellite observations, but may not fully capture the underlying meteorological drivers of drought development. The combination of these two indices enables a more holistic understanding of agricultural drought by linking cause and effect where SPI identifies precipitation deficits as the meteorological trigger, and VHI reveals the resulting vegetation stress and crop health impacts (Javed et al., 2021). This integrated approach is particularly valuable for rice paddy systems, where crop growth stages have varying sensitivities to both water availability and thermal conditions (Sholihah et al., 2016).

Drought is a recurrent hydroclimatic hazard that significantly affects agricultural productivity, water resources, and ecosystem stability, particularly in tropical regions characterized by high climate variability (Rahmi & Dimyati, 2021). Indonesia, drought events are strongly influenced by seasonal monsoon dynamics and large scale climate phenomena such as the El Niño Southern Oscillation (ENSO), which alter rainfall distribution and increase the vulnerability of rainfed agricultural systems (Turkington et al., 2019). As a

major rice producing region, Sragen Regency in Central Java is highly dependent on stable precipitation patterns, making it particularly sensitive to prolonged dry season anomalies.

Various drought monitoring approaches have been developed using meteorological and remote sensing based indices. The standardized precipitation index is widely recognized for its effectiveness in detecting meteorological drought due to its multi temporal flexibility and statistical robustness (Prasetyo et al., 2021). Meanwhile, satellite derived indices such as the VHI have been increasingly utilized to assess agricultural drought by integrating vegetation vigor and thermal stress responses. Previous studies have demonstrated that combining meteorological and vegetation based indicators provides a more comprehensive representation of drought conditions compared to single index approaches (Rahmi & Dimyati, 2021). However, most drought studies in Indonesia still rely on single source data or short term analyses, which limits the understanding of spatio temporal drought variability at the regional scale. In addition, limited research has specifically examined the integration of long term precipitation datasets with multi temporal remote sensing indices to assess both meteorological and agricultural drought simultaneously, particularly at the regency level such as Sragen (Siswanto et al., 2022). This limitation results in insufficient spatial characterization of drought severity and its relationship with agricultural impacts.

Therefore, this study aims to analyze the spatio temporal drought patterns in Sragen Regency by integrating the standardized precipitation index derived from long term CHIRPS rainfall data with EVI based vegetation health index and temperature condition index (TCI) derived from multi temporal Landsat imagery during the dry season. This approach is intended to provide a more comprehensive assessment of drought dynamics by combining meteorological and vegetation based indicators. The expected contribution of this study is to support a more consistent interpretation of drought impacts on agricultural productivity in a rice dominated agricultural region.

MATERIALS AND METHODS

Reseach area

Sragen Regency is located at coordinates 7°15'–7°30' South Latitude and 110°45' – 111°10' East Longitude. This area is in the Bengawan Solo River basin, which flows eastward. Most of the region is lowland with an elevation ranging from 70–480 meters above sea level. The northern part consists of hilly areas that are part of the Kendeng Mountain complex. A small part of the southern region consists of hills that are the foothills of Mount Lawu.

Sragen Regency consists of 20 subdistricts, 208 villages, 2,519 hamlets, and 5,228 neighborhood associations (RT) with a total area of 94,155 hectares. Plupuh and Tanon subdistricts have the most villages, with 16 villages each. Gesi, Tangen, and Jenar subdistricts have the fewest villages, with only 7 villages each.

Sragen has a tropical climate with daily temperatures ranging from 19 to 31ºC. This area has an average annual rainfall of less than 3000 mm with no more than 150 rainy days per year. The hydrological conditions of Sragen Regency are characterized by the presence of various rivers that flow within the Bengawan Solo River Basin (DAS) and the Jratunseluna River Basin (a combination of the Jragung, Tuntang, Serang, Lusi, and Juana rivers). The waterways included in the Bengawan Solo River Basin include the Mungkung, Kenatan, Jenar, Kedungaren, Tanggan, Teseh, and Kedung Dowo rivers, while the Jratunseluna River Basin includes the Serang River.

Methodology

This study employed a comprehensive remote sensing and meteorological analysis framework to assess rice paddy drought conditions in Sragen Regency across three distinct climatic periods: El Niño (2015), normal conditions (2018), and La Niña (2022). The research workflow was systematically designed to integrate satellite derived vegetation health indices with precipitation-based drought indicators to characterize spatiotemporal patterns of agricultural drought and their impacts on rice productivity. The investigation commenced with extensive observation and literature studies to establish the theoretical foundation and identify appropriate methodological approaches. Research tools and materials were subsequently prepared, encompassing both satellite imagery and meteorological datasets. Monthly satellite images are used in the peak dry conditions from June to October, unfortunately the 2022 satellite data for October is unavailable due to the highly cloud coverage that will affect the entirety of the

research purposes. Landsat 8 imagery for 2015 and 2018, and Landsat 9 imagery for 2022 were acquired as primary data sources for vegetation health assessment. These images underwent rigorous preprocessing, including cropping to the study area boundary, radiometric correction to ensure data consistency, and conversion from digital number (DN) to top of atmosphere (TOA) reflectance and radiance values following standard Landsat calibration procedures (Danang et al., 2014). For meteorological drought assessment, monthly precipitation data spanning 1993–2023 were obtained and processed through the Climate Hazards Group InfraRed Precipitation with Station data (CHIRPS) dataset (Funk et al., 2015). This extensive temporal coverage enabled robust calculation of precipitation anomalies and establishment of climatological baselines. Additionally, rice planting area, harvest area, and productivity datasets were compiled to facilitate validation of drought impacts on actual agricultural output.

The VHI was derived through a multi-step process involving several intermediate indices (F. N. Kogan, 1995). Following atmospheric correction using the Fast Line-of-sight Atmospheric Analysis of Spectral Hypercubes (FLAASH) algorithm (ENVI, 2009). Vegetation condition was evaluated using the Enhanced Vegetation Index (EVI), which improves sensitivity in high biomass regions and reduces atmospheric and soil background effects compared to NDVI (Amalo et al., 2017). EVI was derived from Landsat surface reflectance data using the following equation:

$$EVI = G \times \frac{(NIR - Red)}{(NIR + C_1 \times Red - C_2 \times Blue + L)} \quad (1)$$

where: NIR, Red, and Blue represent the reflectance of near infrared, red, and blue bands in Landsat satellite images, respectively G is the gain factor (2.5), $C1$ and $C2$ are aerosol resistance coefficients (6 and 7.5), and L is the canopy background adjustment factor (Huete et al., 2002).

Vegetation condition index was computed by normalizing EVI values against their long-term minimum and maximum values, thereby quantifying vegetation conditions relative to historical ranges (Amalo et al., 2018). The VCI formula is expressed as,

$$VCI = \frac{(EVI_\alpha - EVI_{min})}{(EVI_{max} - EVI_{min})} \times 100 \quad (2)$$

where: $EVI\alpha$ is the EVI value at a given time, and $EVI\ min$ and $EVI\ max$ represent the minimum and maximum EVI values during the study period.

Lower VCI values indicate higher vegetation stress and potential agricultural drought conditions. Thermal components were extracted through a parallel processing chain (F. N. Kogan, 1997). Brightness temperature (BT) was derived from thermal infrared bands, followed by calculation of the proportion of vegetation (PV) and land surface emissivity (F. N. Kogan, 1995). Land surface temperature (LST) was then retrieved using established algorithms that account for atmospheric effects and surface emissivity variations (F. N. Kogan, 1997). LST is a critical parameter for detecting thermal stress associated with drought conditions (Weng et al., 2004). Subsequently, brightness temperature and land surface temperature is calculated as,

$$BT = \frac{K2}{ln(\frac{K_1}{L_\lambda} + 1)} \quad (3)$$

where: $K1$ and $K2$ are band-specific thermal conversion constants provided in the Landsat metadata, and $L\lambda$ is the top of atmosphere spectral radiance.

The resulting BT is expressed in Kelvin (K) (Weng et al., 2004).

$$LST = \frac{BT}{1 + ln\left(\frac{\lambda \times BT}{\rho}\right) ln(\epsilon)} \quad (4)$$

Table 1. Statistical rice stages in Sragen Regency

Rice cultivation, harvest, production and productivity in Sragen Regency			
Rice Stages	Year		
	2015	2018	2022
Cultivation (ha)	98,145	101,482	108,610
Harvest (ha)	97,444	100,491	106,933
Production (Ton)	628,743	634,454	678,575
Productivity (ha/Ton)	6.45	6.31	6.35

Note: data achieved from the Sragen Regency Food Security, Agriculture, and Fisheries Agency.

where: BT is the brightness temperature (K), λ is the effective wavelength of the thermal band in Landsat, ρ is a constant derived from Planck's law, and ε represents land surface emissivity (Sobrino et al., 2004).

Emissivity was estimated using a vegetation based approach derived from the enhanced vegetation index (EVI) to ensure consistency with the vegetation indicator used for drought assessment.

The temperature condition index (TCI) was subsequently computed by normalizing LST values against their historical extremes, representing thermal stress conditions (Bento et al., 2020). The TCI formula is expressed as:

$$TCI = \frac{(LST_{max} - LST_{\alpha})}{(LST_{max} - LST_{min})} \times 100 \quad (5)$$

where: $LST\alpha$ denotes land surface temperature at a specific time, while $LST\ max$ and $LST\ min$ represent the maximum and minimum LST values within the observation period.

The final VHI was synthesized by integrating VCI and TCI with equal weighting (α) of 0.5 (F. N. Kogan, 2001), providing a composite indicator that captures both vegetation vigor and thermal stress conditions. The VHI formula is expressed as:

$$VHI = \alpha VCI + (1 - \alpha)TCI \quad (6)$$

where: α is the weighting coefficient, commonly set to 0.5, assuming equal contributions of vegetation and temperature conditions (Bento et al., 2018).

Lower VHI values indicate severe to extreme drought stress, while higher values reflect healthier vegetation conditions. VHI values were classified according to the Kogan VHI classification (F. Kogan, 2002), ranging from extreme drought (VHI < 10) to no drought conditions (VHI > 40).

The SPI was calculated using the comprehensive CHIRPS precipitation dataset spanning three decades (1993–2023) (Funk et al., 2015). Monthly precipitation data underwent interpolation to ensure spatial continuity across the study area. SPI values were computed at multiple temporal scales, with particular emphasis on the 5-month SPI (SPI-5) to capture medium term precipitation deficits relevant to rice growing seasons (Fentaw et al., 2023). The SPI calculation followed the standard methodology involving fitting of precipitation data to a gamma probability distribution, followed by transformation to a normal distribution (Mckee et al., 1993). The SPI formula is expressed as:

$$SPI = \frac{(X_{ij} - X_{im})}{\sigma} \quad (7)$$

where: Xij represents precipitation at a given time, Xim is the long term mean precipitation, and σ is the standard deviation.

Resulting SPI values were than classified according to USDM categories, with negative values indicating drought conditions and positive values representing wet conditions (Mckee et al., 1993). Both VHI and SPI outputs underwent rigorous validation procedures. VHI results were validated against rice productivity datasets to assess the correspondence between remotely sensed vegetation stress and actual yield impacts. SPI values were validated through comparison with observed precipitation patterns and known drought events documented in historical records. Cross validation between VHI and SPI provided additional confidence in the drought characterization, as these indices derived from independent data sources should exhibit spatial and temporal concordance during drought episodes.

The validated VHI and SPI datasets for 2015, 2018, and 2022 were integrated with land use maps to conduct comprehensive spatial analysis of rice paddy drought patterns. Geographic information system (GIS) techniques were employed to overlay drought indices with rice cultivation areas, enabling identification of vulnerable zones and quantification of drought affected areas (Rao et al., 2017). Temporal comparisons across the three study years facilitated assessment of how different climatic conditions influenced drought severity, spatial extent, and agricultural impacts (Alahacoon & Amarnath, 2022).

Table 2. VHI drought classification

VHI value	Drought category
0 – 10	Extreme drought
10 – 20	Severe drought
20 – 30	Moderate drought
30 – 40	Mild drought
>40	No drought

Table 3. SPI drought classification

SPI drought classification table (USDM)			
SPI Range	USDM category	Classification	Description
1.91 to 2.5+	W4	Exceptional wet	Exceptionally wet conditions
1.51 to 1.9	W3	Extremely Wet	Extremely wet conditions
1.21 to 1.5	W2	Severe Wet	Severely wet condition
0.71 to 1.2	W1	Moderately Wet	Moderately wet conditions
0.5 to 0.7	W0	Abnormally Wet	Abnormally wet conditions
-0.5 to -0.7	D0	Abnormally Dry	Going into or coming out of drought
-0.71 to -1.2	D1	Moderate Drought	Some damage to crops and pastures
-1.21 to -1.5	D2	Severe Drought	Crop or pasture losses likely
-1.51 to -1.9	D3	Extreme Drought	Major crop/pasture losses
-2.0 to -2.5	D4	Exceptional Drought	Exceptional and widespread losses

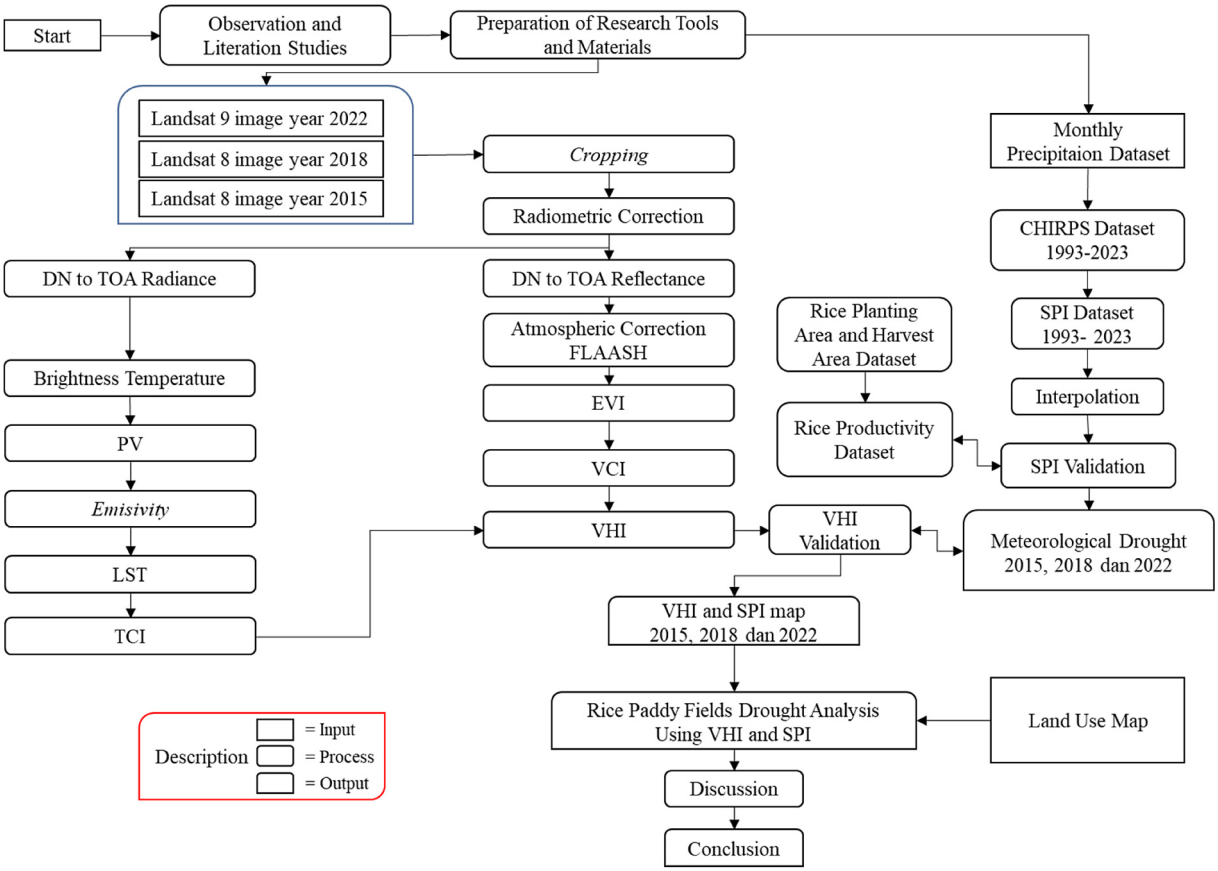

Figure 1. Methodological flowcart for modelling spatial and temporal drought

RESULTS AND DISCUSSION

The analysis of VHI across three distinct climatic periods revealed substantial variability in rice paddy drought conditions in Sragen Regency. El Niño 2015 demonstrated the most severe agricultural drought, with areas experiencing extreme drought (VHI < 10) expanding from 488.43 ha in June to 5,040.50 ha by October a more than tenfold increase. Severe drought areas (VHI 10–20) exhibited an even more dramatic escalation, from 3,292.99 ha to 11,560.39 ha, with the most pronounced intensification occurring between August and October. The spatial distribution analysis indicated that drought conditions were pervasive across the regency, with particularly severe impacts concentrated in the eastern, northern, and central regions. By October 2015, approximately

Table 4. VHI are width Kogan classification

Year	Month	VHI area width (ha)					
		Extreme drought	Severe drought	Moderate drought	Mild drought	No drought	Cloud
2015	June	488.43	3,292.99	8,221.44	13,106.64	48,252.98	-
	July	741.62	2,789.01	10,949.17	16,423.72	40,588.70	1,870.27
	August	1,851.38	6,262.63	11,191.43	13,113.73	40,870.16	73.16
	September	3,011.65	9,617.22	13,284.09	11,652.78	34,898.96	897.78
	October	5,040.50	11,560.39	13,218.34	14,743.84	27,148.14	1,651.27
2018	June	512.91	2,260.29	6,591.29	15,280.27	48,717.64	0.09
	July	638.51	2,050.94	8,392.64	19,792.23	42,487.98	0.18
	August	1,648.93	3,932.08	7,998.55	12,327.16	47,455.23	0.54
	September	2,692.81	6,955.12	11,802.79	12,200.84	34,775.36	4,935.56
	October	2,359.01	13,687.83	20,480.18	17,816.38	17,176.93	1,842.16
2022	June	256.34	583.38	1,581.00	3,352.49	66,579.49	1,009.80
	July	28.43	614.30	5,448.89	8,820.58	58,449.48	0.81
	August	324.87	656.60	1,821.83	5,295.68	65,263.14	0.36
	September	311.68	920.48	2,541.18	6,053.23	63,535.92	-

63% of the total area (46,214.86 ha) experienced varying degrees of drought stress, leaving only 27,148.14 ha (37%) in non-drought conditions.

In contrast, the normal year 2018 presented a paradoxical drought pattern that challenges conventional assumptions about climate classification. Despite the absence of extreme climate phenomena, extreme drought areas increased from 512.91 ha in June to 2,692.81 ha in September, while severe drought expanded dramatically to 13,687.83 ha by October. The non-drought area declined precipitously from 48,717.64 ha (66.4%) in June to merely 17,176.93 ha (23.4%) in October, indicating more extensive agricultural stress than initially anticipated for a climatically normal year. Spatial analysis revealed that while drought initiation was more localized compared to 2015, the subsequent expansion was remarkably rapid, particularly affecting eastern and northern agricultural zones that demonstrated heightened vulnerability to precipitation deficits.

The La Niña year 2022 exhibited markedly different characteristics, with vegetation health remaining predominantly robust throughout the observation period. Extreme drought areas remained minimal, ranging only from 256.34 ha to 324.87 ha, while severe drought peaked at 920.48 ha in September substantially lower than both 2015 and 2018. Critically, non-drought areas maintained consistently high coverage, fluctuating between 58,449.48 ha (79.7%) and 66,579.49 ha (90.8%) across the monitoring period. The spatial

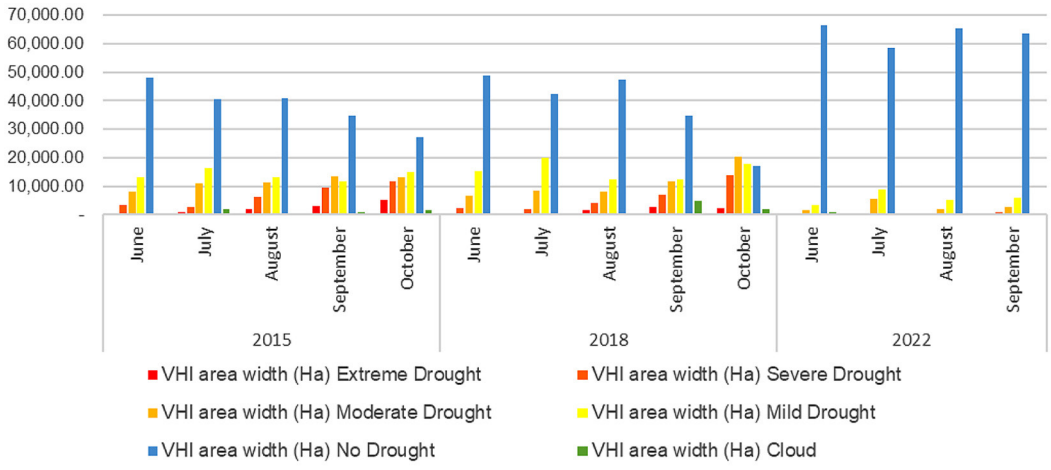

Figure 2. VHI Kogan classification area width graph

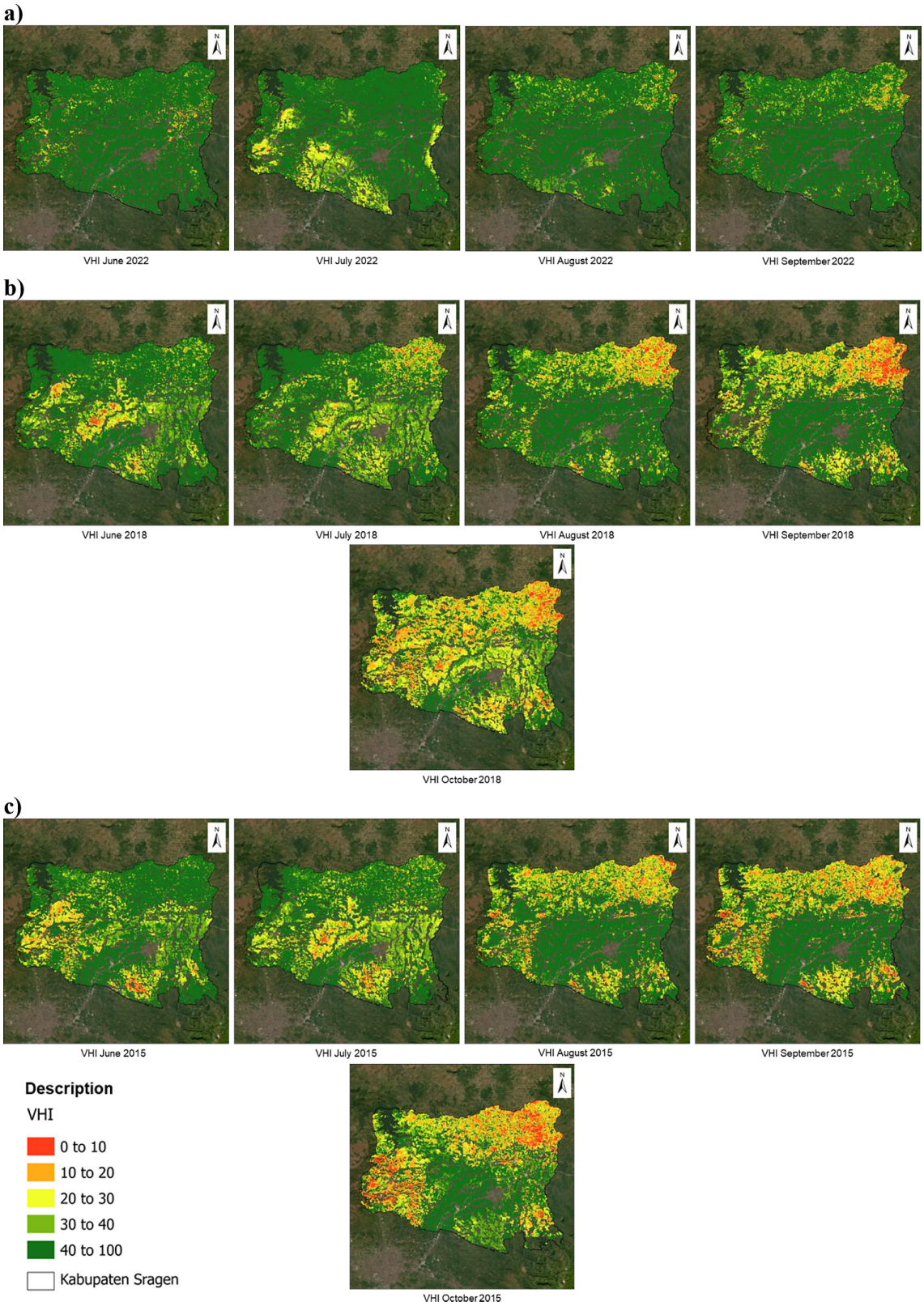

Figure 3. Sragen regency monthly spatiotemporal VHI map (c) 2015 (El Nino), (b) 2018 (Normal) and (a) 2022 (La Nina)

distribution demonstrated that drought stress, when present, was largely confined to the eastern and southeastern sectors, with western regions proximate to water bodies maintaining healthy vegetation conditions throughout the season. This spatial pattern underscores the protective influence of existing water infrastructure and natural water resources during favorable climatic conditions.

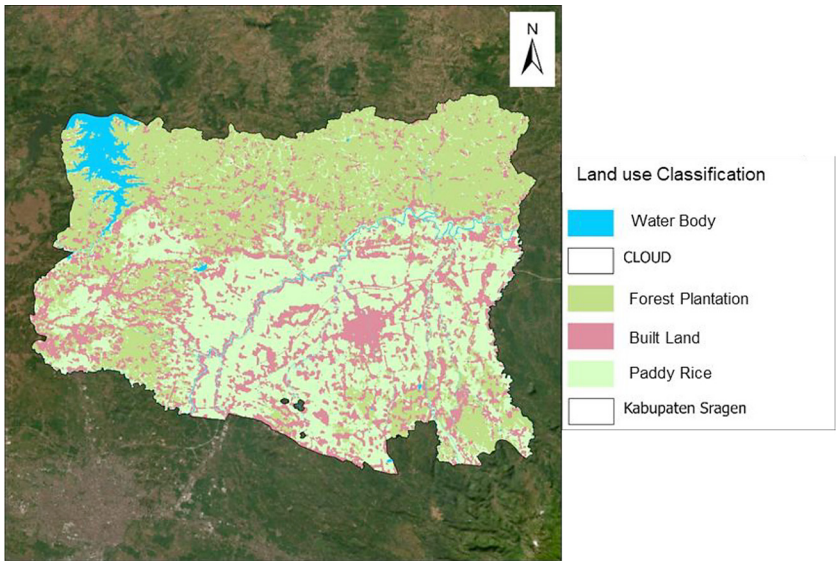

Figure 4. Sragen regency land use map

Meteorological drought characteristics and precipitation dynamics

SPI analysis at the 5-month scale (SPI-5) provided crucial insights into the meteorological drivers underlying the observed vegetation stress patterns. The El Niño year 2015 was characterized by persistently negative SPI-5 values ranging from -2.5 to -1.6 across most of the regency, classifying the period as experiencing extreme to exceptional drought (D3-D4 categories) according to USDM standards. Monthly precipitation data corroborated these findings, revealing critically low rainfall during the June-October period, with values plummeting to 13.38-28.39 mm per month, far below the threshold necessary to support rice cultivation (Luo et al., 2022). This severe precipitation deficit, occurring during critical rice growth stages including flowering and grain filling, created cumulative water stress that persisted despite relatively high rainfall in the preceding months (January-April totaling >1,000 mm) and subsequent months (November-December totaling 572.35 mm).

The 2018 precipitation pattern exhibited extreme temporal variability that explains the unexpectedly severe drought impacts despite normal climate classification. SPI-5 values predominantly ranged from -1.29 to -0.8, indicating moderate drought conditions (D0-D1 categories). However, monthly precipitation data revealed an acute crisis in July with only 13.91 mm the lowest recorded value across all study years followed by persistently low values through October (71.13 mm in June, 21.63 mm in August, 28.29 mm in September). This midseason precipitation

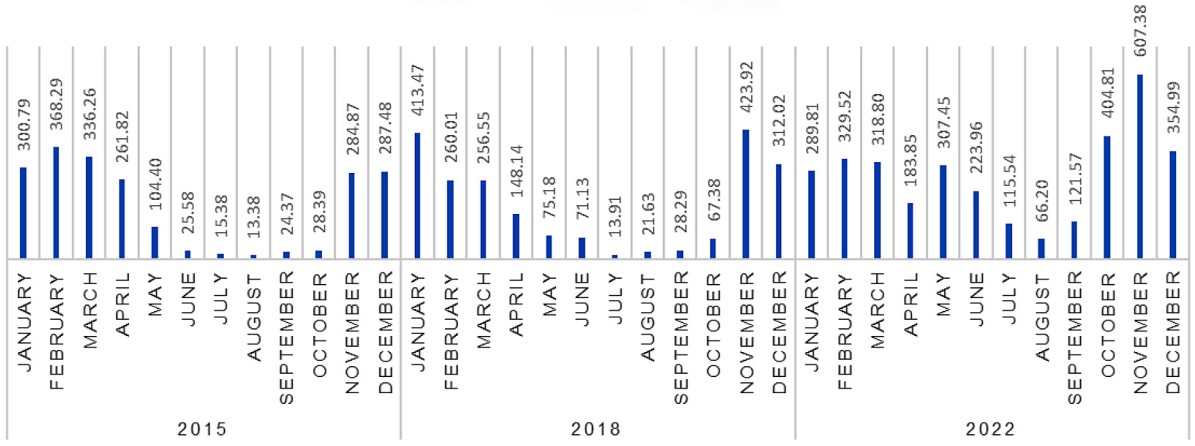

Figure 5. Precipitation graph Sragen regency

collapse, occurring after adequate early-year rainfall (January-March totaling >900 mm), created a critical water deficit during peak crop water demand periods. The delayed onset of substantial rainfall (423.92 mm in November, 312.02 mm in December) arrived too late to prevent accumulated agricultural stress, explaining the extensive drought affected areas observed in VHI analysis.

La Niña 2022 demonstrated contrasting meteorological conditions with predominantly positive SPI-5 values (1.201-1.5) across the regency, classifying the period as extremely wet (W3 category). Monthly precipitation analysis revealed consistently adequate to abundant rainfall throughout the critical growing season, with June-September values ranging from 66.20 mm to 223.96 mm. The early-year period (January-May) accumulated >1,400 mm, providing substantial soil moisture reserves, while peak rainfall occurred in November (607.38 mm) followed by high values in October (404.81 mm) and December (354.99 mm). This well distributed precipitation pattern,

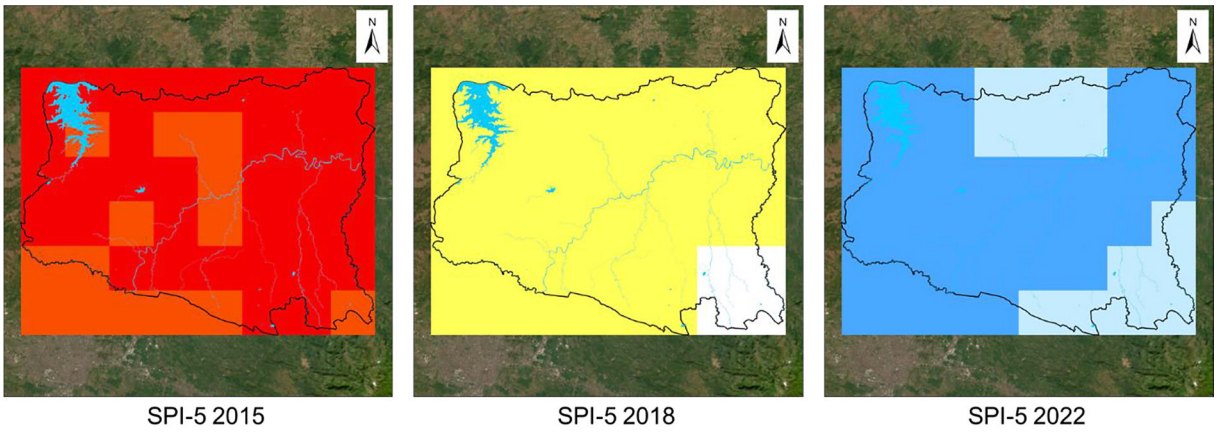

Figure 6. Sragen regency yearly spatiotemporal SPI-5 map 2015 (El Nino), 2018 (Normal) and 2022 (La Nina)

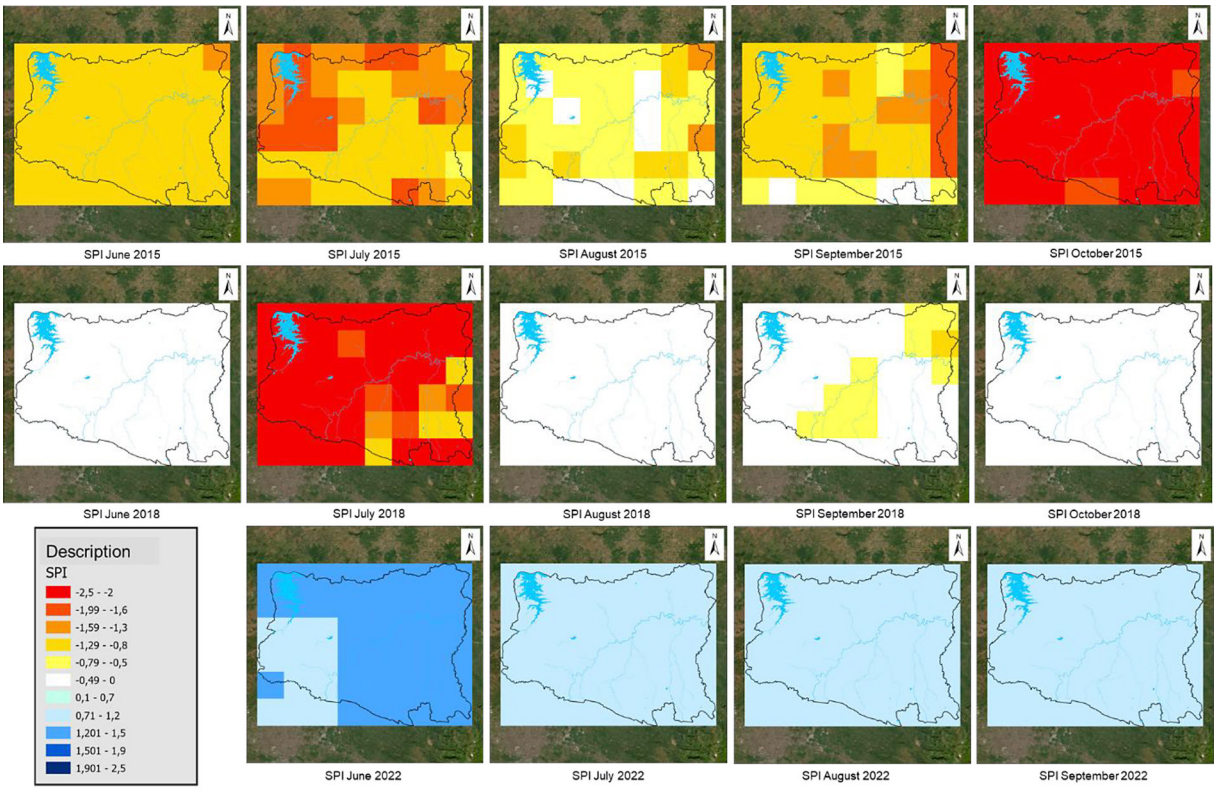

Figure 7. Sragen regency monthly spatiotemporal SPI-1 map 2015 (El Nino), 2018 (Normal) and 2022 (La Nina)

characteristic of La Niña influence, maintained adequate soil moisture throughout rice phenological stages, explaining the minimal drought stress and optimal vegetation health indices observed throughout the monitoring period.

Correlation between drought indices and agricultural productivity

The integration of VHI and SPI-5 data with actual rice productivity statistics revealed complex relationships between climatic stress and agricultural outcomes. Contrary to expectations based solely on drought severity indices, the 2015 harvest yielded 628,743 tons with productivity of 6.45 ton/ha surprisingly higher than 2014 (585,503 tons, 5.85 ton/ha) despite experiencing the most extreme meteorological and agricultural drought conditions. This apparent paradox can be attributed to several mitigating factors. First, the presence of substantial reservoir infrastructure and irrigation networks in Sragen Regency provided critical water supplementation during the acute drought period, partially compensating for precipitation deficits (Zhang et al., 2020). Second, the timing of extreme drought onset (intensifying from August onward) may have missed the most sensitive early phenological stages for some rice cultivation cycles, particularly in areas with staggered planting schedules. Third, farmers likely implemented adaptive measures including increased reliance on irrigation, adjustment of planting dates, and prioritization of water allocation to productive fields, thereby maintaining yields despite challenging conditions. The 2018 productivity data (634,454 tons, 6.31 ton/ha) similarly exceeded expectations given the extensive drought-affected areas, though showing slight decline from 2017 (647,263 tons, 6.32 ton/ha). This relatively stable productivity despite 76.6% of the area experiencing drought stress by October further emphasizes the critical buffering role of irrigation infrastructure. However, the spatial analysis revealed that eastern and northern zones areas with historically limited irrigation access experienced more substantial yield reductions, though these localized impacts were partially masked in aggregate statistics. The July precipitation crisis (13.91 mm) occurred during a transitional period between planting cycles for many farmers, potentially reducing its impact on the primary harvest while significantly affecting secondary or delayed plantings.

The La Niña year 2022 achieved the highest recorded production (678,575 tons) though productivity (6.35 ton/ha) was marginally lower than 2015, reflecting the influence of favorable moisture conditions throughout the growing season. The consistently high VHI values and positive SPI-5 indices translated into optimal crop development with minimal stress induced yield losses. Notably, the 2023 data showed a curious pattern with productivity increasing to 6.49 ton/ha yet total production remaining nearly static (678,940 tons) due to reduced harvest area (104,660 ha versus 106,933 ha in 2022), suggesting possible land use changes or delayed planting schedules influenced by residual La Niña effects or other socioeconomic factors.

Rice productivity in Sragen Regency exhibits noticeable interannual variability that generally corresponds with the observed drought patterns during the dry season. Years characterized by higher drought severity, particularly those

Table 5. Rice productivity in Sragen Regency

Rice harvest area and production in sragen regency										
Harvested area (ha)										
Year										
2013	2014	2015	2016	2017	2018	2019	2020	2021	2022	2023
100,044	100,061	97,444	102,183	102,466	100,491	102,744	103,629	108,199	106,933	104,660
Production (Ton)										
Year										
2013	2014	2015	2016	2017	2018	2019	2020	2021	2022	2023
601,040	585,503	628,743	654,709	647,263	634,454	649,015	668,553	703,458	678,575	678,940
Productivity (Ton/ha)										
Year										
2013	2014	2015	2016	2017	2018	2019	2020	2021	2022	2023
6.01	5.85	6.45	6.41	6.32	6.31	6.32	6.45	6.50	6.35	6.49

associated with lower SPI values and reduced vegetation health, tend to show a decline in harvested area and productivity. This pattern suggests that precipitation deficits and increased thermal stress play a significant role in influencing agricultural performance in predominantly rice based systems.

The spatial comparison indicates that sub districts with stronger vegetation stress (lower VHI and EVI values) tend to coincide with areas experiencing reduced rice productivity. This relationship highlights the sensitivity of rice cultivation to moisture availability and surface temperature conditions during critical growth periods. However, the decline in productivity is not uniformly distributed across the region, indicating that local irrigation infrastructure and water management practices may mitigate the direct impacts of meteorological drought such as the availability of reservoir in the region.

Furthermore, the relatively stable productivity observed in certain years despite moderate drought signals suggests the presence of adaptive agricultural practices, such as irrigation scheduling and cropping adjustments, which can buffer drought impacts. This finding implies that agricultural resilience in Sragen Regency is not solely controlled by climatic variability but also influenced by management and technological interventions in rice farming systems such as irrigation systems.

Overall, the integration of drought indices and agricultural statistics demonstrates that severe drought conditions are generally associated with decreased rice productivity, although the relationship is not strictly linear. This non linear response reflects the combined influence of climatic stress, irrigation availability, and local agronomic practices, emphasizing the importance of integrated drought monitoring for sustainable agricultural planning in Sragen Regency.

CONCLUSIONS

This study demonstrates that the integration of SPI and EVI based VHI provides a consistent framework for assessing spatio temporal drought dynamics in Sragen Regency during the dry season. The multi temporal analysis indicates that drought severity varies interannually, with stronger meteorological deficits reflected in reduced vegetation health and increased surface thermal stress. The spatial patterns reveal that drought impacts are more pronounced in rainfed agricultural areas, while irrigated zones exhibit relatively stable vegetation conditions despite precipitation variability.

The comparison between drought indices and rice productivity suggests a general correspondence between higher drought intensity and fluctuations in agricultural performance, although the response is not uniform across years. This indicates that climatic stress interacts with irrigation availability and local agricultural management, resulting in a non linear relationship between drought indicators and productivity outcomes.

Methodologically, the use of long term CHIRPS precipitation data combined with Landsat derived EVI and emissivity corrected LST improves the reliability of drought characterization by capturing both meteorological and agricultural dimensions. The findings confirm that single index approaches may not fully represent drought impacts in heterogeneous agricultural landscapes.

Overall, the integrated SPI, EVI and VHI approach provides a spatially explicit basis for drought monitoring and supports more informed agricultural mitigation strategies in climate sensitive rice producing regions such as Sragen Regency. Future studies should incorporate higher temporal resolution data and irrigation-specific variables to enhance the accuracy of drought impact assessment and agricultural resilience evaluation.

Acknowledgements

The authors express sincere gratitude to the Universitas Gadjah Mada Graduate School for financial support through the Graduate School Research Grants 2025, which made this research possible. We acknowledge the invaluable assistance of faculty members and laboratory staff who provided guidance and technical support throughout the study. Our appreciation extends to the relevant agencies for providing access to satellite imagery, meteorological data, and agricultural statistics essential for this research. We also thank the local agricultural offices in Sragen Regency for their cooperation in data collection and validation processes. This research was funded by the Universitas Gadjah Mada Graduate School Research Grants 2025.

REFERENCES

1. Alahacoon, N., & Amarnath, G. (2022). Agricultural drought monitoring in Sri Lanka using multisource satellite data. *Advances in Space Research*, *69*(11),

4078–4097. https://doi.org/10.1016/j.asr.2022.03.009

2. Amalo, L. F., Hidayat, R., & Haris. (2017). Comparison between remote-sensing-based drought indices in East Java. *IOP Conference Series: Earth and Environmental Science*, *54*(1). https://doi.org/10.1088/1755-1315/54/1/012009
3. Amalo, L. F., Hidayat, R., & Sulma, S. (2018). Analysis of agricultural drought in east java using vegetation health index. *Agrivita*, *40*(1), 63–73. https://doi.org/10.17503/agrivita.v40i1.1080
4. Asmall, T., Abrams, A., Röösli, M., Cissé, G., Carden, K., & Dalvie, M. A. (2021). The adverse health effects associated with drought in Africa. *Science of The Total Environment*, *793*, 148500. https://doi.org/10.1016/j.scitotenv.2021.148500
5. Awasthi, R., Devi, P., Jha, U. C., Sharma, K. D., Roorkiwal, M., Kumar, S., Pareek, A., Siddique, K. H. M., Prasad, P. V., Parida, S. K., & Nayyar, H. (2024). Exploring the synergistic effects of drought and heat stress on chickpea seed development: Insights into nutritional quality and seed yield. *Plant Stress*, *14*, 100635. https://doi.org/10.1016/j.stress.2024.100635
6. Bajrai, L. H. (2025). The ENSO effect: Climate variability, disease ecology, and implications for mass gathering events. *Mass Gathering Medicine*, *4*, 100039. https://doi.org/10.1016/j.mgmed.2025.100039
7. Bento, V. A., Gouveia, C. M., DaCamara, C. C., Libonati, R., & Trigo, I. F. (2020). The roles of NDVI and Land Surface Temperature when using the Vegetation Health Index over dry regions. *Global and Planetary Change*, *190*. https://doi.org/10.1016/j.gloplacha.2020.103198
8. Bento, V. A., Gouveia, C. M., DaCamara, C. C., & Trigo, I. F. (2018). A climatological assessment of drought impact on vegetation health index. *Agricultural and Forest Meteorology*, *259*, 286–295. https://doi.org/10.1016/j.agrformet.2018.05.014
9. Bhaga, T. D., Dube, T., Shekede, M. D., & Shoko, C. (2023). Investigating the effectiveness of Landsat-8 OLI and Sentinel-2 MSI satellite data in monitoring the effects of drought on surface water resources in the Western Cape Province, South Africa. *Remote Sensing Applications: Society and Environment*, *32*. https://doi.org/10.1016/j.rsase.2023.101037
10. Danang, R. *, Candra, S., Universitas,), Soedirman, J., Teknologi, P., Data, D., & Jauh, P. (2014). Koreksi radiometrik citra landsat-8 kanal multispektral menggunakan top of atmosphere (TOA) untuk mendukung klasifikasi penutup lahan. In: *Prosiding Seminar Nasional Penginderaan Jauh*. https://karya.brin.go.id/id/eprint/10914/
11. ENVI. (2009). *Atmospheric Correction Module: QUAC and FLAASH User's Guide 20AC47DOC*. www.apache.org/
12. Fentaw, A. E., Yimer, A. A., & Zeleke, G. A. (2023). Monitoring spatio-temporal drought dynamics using multiple indices in the dry land of the upper Tekeze Basin, Ethiopia. *Environmental Challenges*, *13*. https://doi.org/10.1016/j.envc.2023.100781
13. Funk, C., Peterson, P., Landsfeld, M., Pedreros, D., Verdin, J., Shukla, S., Husak, G., Rowland, J., Harrison, L., Hoell, A., & Michaelsen, J. (2015). The climate hazards infrared precipitation with stations—a new environmental record for monitoring extremes. *Scientific Data*, *2*(1), 150066. https://doi.org/10.1038/sdata.2015.66
14. Gebre, B., Ayenew, H. Y., & Biadgilign, S. (2021). Drought, hunger and coping mechanisms among rural household in Southeast Ethiopia. *Heliyon*, *7*(3), e06355. https://doi.org/10.1016/j.heliyon.2021.e06355
15. Guttman, N. B. (1999). Accepting the standardized precipitation index: A calculation algorithm. *Journal of the American Water Resources Association*, *35*(2), 311–322. https://doi.org/10.1111/j.1752-1688.1999.tb03592.x
16. Huete, A., Didan, K., Miura, T., Rodriguez, E. P., Gao, X., & Ferreira, L. G. (2002). Overview of the radiometric and biophysical performance of the MODIS vegetation indices. *Remote Sensing of Environment*, *83*(1–2), 195–213. https://doi.org/10.1016/S0034-4257(02)00096-2
17. Javed, T., Li, Y., Rashid, S., Li, F., Hu, Q., Feng, H., Chen, X., Ahmad, S., Liu, F., & Pulatov, B. (2021). Performance and relationship of four different agricultural drought indices for drought monitoring in China's mainland using remote sensing data. *Science of the Total Environment*, *759*. https://doi.org/10.1016/j.scitotenv.2020.143530
18. Junior, R. R. H. (2002). A review of twentieth-century drought indices used in the United States. *Bulletin of the American Meteorological Society*, *83*(8), 1149–1165. https://doi.org/10.1175/1520-0477(2002)083<1149:AROTDI>2.3.CO;2
19. Kogan, F. (2002). World droughts in the new millennium from AVHRR-based vegetation health indices. *Eos, Transactions American Geophysical Union*, *83*(48), 557–563. https://doi.org/10.1029/2002EO000382
20. Kogan, F. N. (1995). Application of vegetation index and brightness temperature for drought detection. *Advances in Space Research*, *15*(11), 91–100. https://doi.org/10.1016/0273-1177(95)00079-T
21. Kogan, F. N. (1997). Global drought watch from space. *American Meteorological Society*, *78*(4), 621–636. https://doi.org/https://doi.org/10.1175/1520-0477(1997)078%3C0621:GDWFS%3E2.0.CO;2
22. Kogan, F. N. (2001). Operational space technology for Global vegetation assessment. *Bulletin of the American Meteorological Society*, *82*(9), 1949–1964. https://doi.

org/10.1175/1520-0477(2001)082<1949:OSTFGV>2.3.CO;2

23. Letsoalo, N., Samuels, I., Cupido, C., Ntombela, K., Finca, A., Foster, J., Tjelele, J., & Knight, R. (2023). Coping and adapting to drought in semi-arid Karoo rangelands: Key lessons from livestock farmers. *Journal of Arid Environments*, *219*, 105070. https://doi.org/10.1016/j.jaridenv.2023.105070
24. Luo, W., Chen, M., Kang, Y., Li, W., Li, D., Cui, Y., Khan, S., & Luo, Y. (2022). Analysis of crop water requirements and irrigation demands for rice: Implications for increasing effective rainfall. *Agricultural Water Management*, *260*, 107285. https://doi.org/10.1016/j.agwat.2021.107285
25. Mckee, T. B., Doesken, N. J., & Kleist, J. (1993). The relationship of drought frequency and duration to time scales. *Eighth Conference on Applied Climatology*, 17–22.
26. Mupepi, O., & Matsa, M. M. (2023). A combination of vegetation condition index, standardized precipitation index and human observation in monitoring spatio-temporal dynamics of drought. A case of Zvishavane District in Zimbabwe. *Environmental Development*, *45*. https://doi.org/10.1016/j.envdev.2023.100802
27. Piao, S., Ciais, P., Huang, Y., Shen, Z., Peng, S., Li, J., Zhou, L., Liu, H., Ma, Y., Ding, Y., Friedlingstein, P., Liu, C., Tan, K., Yu, Y., Zhang, T., & Fang, J. (2010). The impacts of climate change on water resources and agriculture in China. In *Nature* (Vol. 467, Number 7311, pp. 43–51). Nature Publishing Group. https://doi.org/10.1038/nature09364
28. Prasetyo, S. Y. J., Hartomo, K. D., & Paseleng, M. C. (2021). Satellite imagery and machine learning for identification of aridity risk in central Java Indonesia. *PeerJ Computer Science*, *7*, e415. https://doi.org/10.7717/peerj-cs.415
29. Rahmi, K. I. N., & Dimyati, M. (2021). Remote sensing and GIS application for monitoring drought vulnerability in Indonesia: a review. *Bulletin of Electrical Engineering and Informatics*, *10*(6), 3507–3518. https://doi.org/10.11591/eei.v10i6.3249
30. Rao, M., Silber-Coats, Z., Powers, S., Fox III, L., & Ghulam, A. (2017). Mapping drought-impacted vegetation stress in California using remote sensing. *GIScience & Remote Sensing*, *54*(2), 185–201. https://doi.org/10.1080/15481603.2017.1287397
31. Senay, G. B., Velpuri, N. M., Bohms, S., Budde, M., Young, C., Rowland, J., & Verdin, J. P. (2023). Drought monitoring and assessment. In *Hydro-Meteorological Hazards, Risks, and Disasters* (2nd ed., Vol. 5, pp. 247–276). Elsevier. https://doi.org/10.1016/B978-0-12-819101-9.00002-9
32. Sholihah, R. I., Trisasongko, B. H., Shiddiq, D., Iman, L. O. S., Kusdaryanto, S., Manijo, & Panuju, D. R. (2016). Identification of Agricultural Drought Extent Based on Vegetation Health Indices of Landsat Data: Case of Subang and Karawang, Indonesia. *Procedia Environmental Sciences*, *33*, 14–20. https://doi.org/10.1016/j.proenv.2016.03.051
33. Siswanto, S., Wardani, K. K., Purbantoro, B., Rustanto, A., Zulkarnain, F., Anggraheni, E., Dewanti, R., Nurlambang, T., & Dimyati, M. (2022). Satellite-based meteorological drought indicator to support food security in Java Island. *PLOS ONE*, *17*(6), e0260982. https://doi.org/10.1371/journal.pone.0260982
34. Sobrino, J. A., Jiménez-Muñoz, J. C., & Paolini, L. (2004). Land surface temperature retrieval from LANDSAT TM 5. *Remote Sensing of Environment*, *90*(4), 434–440. https://doi.org/10.1016/j.rse.2004.02.003
35. Turkington, T., Timbal, B., & Rahmat, R. (2019). The impact of global warming on sea surface temperature based El Niño–Southern Oscillation monitoring indices. *International Journal of Climatology*, *39*(2), 1092–1103. https://doi.org/10.1002/joc.5864
36. Uddin, M. J., Hu, J., Islam, A. R. M. T., Eibek, K. U., & Nasrin, Z. M. (2020). A comprehensive statistical assessment of drought indices to monitor drought status in Bangladesh. *Arabian Journal of Geosciences*, *13*(9). https://doi.org/10.1007/s12517-020-05302-0
37. Wang, S., Huang, S., Wang, C., Zhang, X., Wu, J., Gulakhmadov, A., Niyogi, D., & Chen, N. (2025). Global anthropogenic effects on meteorological—hydrological—soil moisture drought propagation: Historical analysis and future projection. *Journal of Hydrology*, *653*, 132755. https://doi.org/10.1016/j.jhydrol.2025.132755
38. Weng, Q., Lu, D., & Schubring, J. (2004). Estimation of land surface temperature–vegetation abundance relationship for urban heat island studies. *Remote Sensing of Environment*, *89*(4), 467–483. https://doi.org/10.1016/j.rse.2003.11.005
39. Yu, W., Shao, M., Ren, M., Zhou, H., Jiang, Z., & Li, D. (2013). Analysis on spatial and temporal characteristics drought of Yunnan Province. *Acta Ecologica Sinica*, *33*(6), 317–324. https://doi.org/10.1016/j.chnaes.2013.09.004
40. Yu, X., & Guo, X. (2023). Inter-annual drought monitoring in northern mixed grasslands by a revised vegetation health index from historical Landsat imagery. *Journal of Arid Environments*, *213*, 104964. https://doi.org/10.1016/j.jaridenv.2023.104964
41. Zeng, J., Zhou, T., Qu, Y., Bento, V. A., Qi, J., Xu, Y., Li, Y., & Wang, Q. (2023). An improved global vegetation health index dataset in detecting vegetation drought. *Scientific Data*, *10*(1). https://doi.org/10.1038/s41597-023-02255-3
42. Zhang, J., Ding, J., Wu, P., Tan, J., Huang, S., Teng, D., Cao, X., Wang, J., & Chen, W. (2020). Assessing arid Inland Lake Watershed Area and Vegetation Response to Multiple Temporal Scales of Drought Across the Ebinur Lake Watershed. *Scientific Reports*, *10*(1). https://doi.org/10.1038/s41598-020-57898-8